

# Long Term Spectral Variability of Seyfert Galaxies from RXTE Color-Flux Diagrams

I. E. Papadakis<sup>1,2</sup>, P. O. Petrucci<sup>3,4</sup>, L. Maraschi<sup>3</sup>, I. M. McHardy<sup>5</sup>, P. Uttley<sup>5</sup>, and F. Haardt<sup>6</sup>

## ABSTRACT

We present results from *RXTE* data obtained during a systematic monitoring program of four Seyfert galaxies (NGC 5548, NGC 5506, MCG -6-30-15 and NGC 4051). We studied the variability of three hardness ratios derived from the light curves in four energy bands (*HR*1, which describes the continuum variations, and *HR*2, *HR*3 which are sensitive to the iron line and reflection component variations with respect to the continuum, respectively). All the objects show similar spectral variations in all ratios. In order to interpret the results we computed the hardness ratios corresponding to a simple spectral model of a power law plus iron line plus reflection component. In order to derive the model *HR*2 and *HR*3 colors, we considered two possibilities: a) variations with constant line equivalent width and reflection parameter  $R$  (the case of a reflecting/reprocessing material that responds with a short delay to the continuum variability) and b) variations with constant line and reflection flux (the case of a reprocessor that does not respond to the fast, intrinsic variations). The overall, mean observed trends can be explained by spectral slope variations ( $\Delta\Gamma \simeq 0.2 - 0.3$ , and  $\simeq 1$  for NGC 4051), and a constant flux Fe line and reflection component, although the existence of a line component which is variable on short time scales cannot be excluded. Finally, we find that the data are not consistent with an increase of  $R$  with flux for individual sources, indicating that, as a single source varies, softer spectra do not correspond to larger  $R$  values.

---

<sup>1</sup>IESL, Foundation for Research and Technology-Hellas, Heraklion, Crete, Greece; e-mail: jhep@physics.uoc.gr

<sup>2</sup>Physics Department, University of Crete, 710 03, Heraklion, Crete, Greece

<sup>3</sup>Osservatorio Astronomico di Brera, Milano, Italy

<sup>4</sup>Laboratoire d' Astrophysique de Grenoble, 38041, Grenoble Cedex 9, France

<sup>5</sup>Department of Physics and Astronomy, University of Southampton, Southampton SO17 1BJ, UK

<sup>6</sup>Universita dell'Insubria, Como, Italy

*Subject headings:* Galaxies: active - Galaxies: nuclei - X-rays: Galaxies - Galaxies: individual(NGC 4051, MCG -6-30-15, NGC 5506, NGC 5548)

## 1. Introduction

X-ray emission is a ubiquitous property of Active Galactic Nuclei (AGN). The spectral characteristics of this emission have been studied in detail the past decade and our understanding of the X-ray emission properties has improved considerably. In general, the X-ray spectra of AGN have a power-law form over a large range in energy. The photon spectral index has a typical value of  $\Gamma \sim 2$  (Nandra & Pounds 1994). Few sources also show a high energy cutoff which can be modeled as an exponential cutoff with e-folding energy of a few 100 keV (Gondek et al. 1996). Furthermore, the presence of the 6.4 keV Fe line and the so-called “Compton reflection hump” indicates the existence of cold, optically thick material that reprocesses and reflects the medium energy X-rays. It is generally believed that this material is located near the primary X-ray source (i.e. the accretion disc). However, this is not the only possibility. The cold material could also be in the form of a torus which is surrounding and obscuring (depending on the inclination) the central nucleus. The existence of this torus is predicted by models that unify Seyfert 1 and 2 galaxies (e.g. Antonucci 1993). The contribution of the torus to the spectrum of Seyfert 1 galaxies (by scattering part of the primary radiation into the line of sight) can in principle explain the reflection bump observed in the spectra of AGN (Ghisellini, Haardt & Matt 1994).

Based on the detailed study of the X-ray spectra of the Seyfert 1 nuclei the currently-popular scenario (the “standard picture” say) is that X-rays from AGN are produced by Compton upscattering of soft photons in a hot “corona” located above the accretion disc (e.g. Haardt & Maraschi 1991, 1993). The X-ray continuum illuminates the disk, which is assumed to be neutral, producing optical/UV emission via reprocessing, the iron line and the reflection hump. Apart from the energy spectra, the X-ray flux and spectral temporal variations can also constrain the emission mechanism. In fact, the spectral variations observed during long, high signal-to-noise observations of NGC 5548 and NGC 7469 (Petruzzi et al. 2000, Nandra et al. 2000) have provided strong support to the Comptonization hypothesis as the origin of X-rays in AGN. In the former case, during a long *Beppo SAX* observation the spectrum became “harder” (i.e. flatter) and the corona temperature decreased together with the [2 – 10] keV flux whereas the total luminosity remained essentially constant. In NGC 7469, simultaneous *RXTE* and *IUE* observations revealed strong X-ray spectral changes which were correlated with the UV flux. In both cases, the observed spectral variations can be naturally explained in terms of thermal Comptonization models since an increase in the UV

photons reduces the temperature of the hot corona and produces a “softer” (i.e. steeper) X-ray power law slope.

In this work we present the results from a spectral variability analysis of four Seyfert galaxies, namely NGC 4051, MCG -6-30-15, NGC 5506 and NGC 5548. These objects have been monitored with *RXTE* on a regular basis since 1996. The main purpose of the observations was to compute accurately the shape of the power density spectrum over a broad range of time scales in order to reveal the existence of characteristic time scales (low or high frequency “breaks”). These time scales can in principle provide model-independent black hole mass estimates through their comparison with similar time scales that have long been identified in the power spectra of Galactic X-ray binaries. The results of this study are presented elsewhere (Uttley, M<sup>c</sup>Hardy & Papadakis 2001). Here we focus on the variability properties of the energy spectra of the sources.

All the sources are strongly variable in the X-rays. MCG -6-30-15 and NGC 5548 are classified as Seyfert 1 nuclei, NGC 5506 is a Seyfert 2 galaxy while NGC 4051 is a Narrow Line Seyfert 1 (NLS1) galaxy. They are typical examples of their class and taken as a whole they can be considered as a representative group of the nearby Seyfert galaxies.

There are two main advantages of the *RXTE* light curves that we study in the present work: *i*) they are of high quality (i.e. high signal to noise ratio) and *ii*) they span regularly a long time interval ( $\sim 3$  years for each source). As a result, we are able to study spectral variations covering the highest, lowest and intermediate flux states over a few years. This is not possible to achieve with the typical X-ray observations of AGN which last for  $\sim$  few days (maximum).

Using the same *RXTE* data, Lamer, M<sup>c</sup>Hardy & Uttley (2000) and Lamer et al. (2001) have already presented a study of the spectral variability of NGC 5506 and NGC 4051. Their study was based on model fitting of flux-averaged energy spectra. In this paper, we follow a different approach. Typically, each source was observed for  $\sim 1$  ksec during each pointing. Although this is not long enough for a direct study of the energy spectrum it allowed us an accurate flux measurement in the [3 – 15] keV band. Using the *RXTE* light curves at different energy bands we computed hardness ratios, produced color-flux diagrams and used these diagrams to investigate the properties of spectral variations. As a result we are able to study the spectral variations in a systematic way, i.e. at each individual observation without considering broad “flux states” for each source. In this way, we cannot investigate whether a given model describes well the energy spectrum of the sources. However, using the simple “power law + iron line + reflection component” model which provides a good representation of the X-ray spectrum of AGN, we were able to study in detail the relationship between the continuum, line flux and reflection component.

The paper is organized as follows. In the following section we present our data and in Section 3 we present the results from the analysis of the variability of the hardness ratios. In Section 4 we use the standard “power law plus reflection component plus narrow iron line” model to compare quantitatively the observed trends in the color-flux diagrams with specific hypothesis on the variability properties. In Section 5 we compare our results with previous studies, and in Sections 6 and 7 we present the discussion of our results and our conclusions.

## 2. Observations and Data reduction

We use data obtained with the PCA on board *RXTE* covering a three year period during observing cycles 1-3 when the PCA gain setting was constant. Details of the data sampling scheme and of the time of the first and last observation of the sources can be found in Uttley et al. (2002). Briefly, the four sources were observed  $\sim 120$  times during the period from April/May 1996 until December 1998/February 1999. Each observation was  $\sim 1$  ksec long and the observing scheme was designed so that the broadest range of time scales would be covered with the minimum observing time. The objects were observed once every week in the first year of the monitoring campaign and then every two weeks. During some periods the monitoring was more intensive (twice daily or daily for a period of two up to four weeks) to sample the shorter time scale variations. The data were reduced using FTOOLS V4.2. We used data from the top layer of the PCUs 0,1,2 only and estimated the background light curves using the *L7* background model (for details see Uttley et al. 2002).

The background subtracted  $[2 - 10]$  keV light curves of the four sources, normalized to their mean, are shown in Figure 1. All are significantly variable. The peak to peak variability amplitude is  $\sim 40, 5, 3$  and  $4$  for NGC 4051, MCG -6-30-15, NGC 5506 and NGC 5548 respectively. Therefore NGC 4051 stands out as the most variable source as is typical of NLS1 nuclei (e.g. Leighly 1999a). During the *RXTE* observations, NGC 4051 went through an unusually “low-state” when the source reached a very low flux level (the period between Day 600 and 750 in Figure 1). In fact, there is the possibility that the central source even “switched-off”, leaving only the reflection spectrum from cold matter to be detected (Guainazzi et al. 1998, Uttley et al. 1999). For that reason, we excluded the points in the NGC 4051 light curves between Day 600 and 750 from the data analysis.

Finally, the *RXTE* observations of NGC 5548 are contaminated by the nearby BL Lac object 1E 1415.6+2557. Chiang et al. (2000) have estimated that the contaminating contribution of this object to the  $2 - 10$  keV NGC 5548 light curves (using the same three PCUs as ours) is  $\sim 2$  counts/sec with a modulation smaller than 0.8 counts/sec. Since we observe a peak to peak count rate difference of  $\sim 20$  counts/sec, the 1E 1415.6+2557 contribution

to the overall variability properties of NGC 5548 should not be crucial.

### 3. Data Analysis

#### 3.1. Hardness Ratios

We extracted light curves in the following energy bands: [3 – 5], [5 – 7], [7 – 10] and [10 – 15] keV. These intervals were chosen so as to separate as much as possible the various emission components in the spectrum of the objects. The first and third band should be representative of the primary continuum mainly, while the iron line and the reflection component emission should contribute in the [5 – 7] keV and [10 – 15] keV bands respectively. From these light curves we calculated three hardness ratios:  $HR1 = C_{7-10keV}/C_{3-5keV}$ ,  $HR2 = C_{7-10keV}/C_{5-7keV}$  and  $HR3 = C_{10-15keV}/C_{7-10keV}$  ( $C_{E1-E2}$  represents the count rate in the energy band  $E1 - E2$ ). These are sensitive to variations : i) of the continuum shape ( $HR1$ ), ii) of the continuum to the iron line ratio ( $HR2$ ) and iii) of the reflection component to the continuum ratio ( $HR3$ ).

Figure 2 shows a plot of the hardness ratios as a function of time since the beginning of the *RXTE* observations for each source. The solid lines show the  $HR$  weighted average values ( $\bar{HR}$ ). These values, together with the root mean square variability amplitude (i.e.  $\sigma_{rms}$ ) of the  $HR$  light curves are reported in Table 1. A constancy  $\chi^2$  test shows that all the  $HR$  values exhibit statistically significant variations, except from the  $HR3$  plot of NGC 5548 for which the significance is only marginal. The  $HR1$  light curve of NGC 4051 has the largest  $\sigma_{rms}$  among the  $HR1$  light curves. This source shows the largest amplitude flux *and* spectral variations.

The main conclusion from Table 1 is that the mean  $HR$  values are roughly similar between the different objects. This implies that the mean energy spectrum has approximately the same spectral shape in all sources. However, there are also some differences. For example, NGC 4051 shows the smallest  $\bar{HR}$  values, indicating that its energy spectrum is softer than the spectrum of the other sources. This is consistent with results from previous studies which have showed that the X-ray energy spectra of NLS1s are “softer” than the spectra of typical S1 galaxies (e.g. Leighly 1999b). The  $\bar{HR}$  values of NGC 5506 (the only S2 source in our sample) are similar to the respective values of NGC 5548 and MCG -6-3015 (the S1 sources in the sample) except from  $\bar{HR}1$ . Its large value is probably due to the presence of a large absorbing column towards that source which causes the energy spectrum to appear “harder” than the spectrum of other sources.

### 3.2. Color-Flux diagrams

Having established the existence of significant spectral variability in all sources, we then investigated whether the spectral variations are correlated with the source flux. Figure 3 shows the plot of  $HR1$  as a function of the normalized  $([3 - 5] + [7 - 10])$  keV count rate ( $C_{(3-5keV+7-10keV)_{norm}}$ ). Figures 4 and 5 show a plot of  $HR2$  and  $HR3$  as a function of the normalized  $[3 - 5]$  keV count rate ( $C_{(3-5keV)_{norm}}$ ). In Figure 3, we have chosen the  $([3 - 5] + [7 - 10])$  keV count rate as representative of the continuum flux, since the sum of the source signal in the two bands should minimize the possibility to introduce artificial correlations due to the inter-dependency of the  $HR1$  and  $C_{(3-5+7-10keV)}$  variables. In Figures 4 and 5, we have used only the  $[3 - 5]$  keV count rate since both  $HR2$  and  $HR3$  are independent of  $C_{(3-5keV)}$ . In all cases, we have normalized the count rates to their mean in order to compare the color-flux plots of the four sources.

The points in the color-flux plots of all the sources cluster in a well defined, “continuous” region rather than forming a scatter diagram or filling separate “islands”. Although it is not clear from the power density spectra of the sources whether we have observed their maximum/minimum flux states with the present *RXTE* observations (see discussion in Uttley et al. 2002) we are certain that we have observed all the “intermediate” flux states of each source between their largest and lowest flux state in the *RXTE* light curves.

The color-flux trends are similar for each object:  $HR1$  systematically decreases (i.e. the energy spectrum softens) as the flux increases. A similar trend is observed for  $HR3$ . On the other hand, the  $HR2$  variations appear to be independent of the source flux.

In order to quantify the above relationships we fitted the data for each galaxy using a power law function of the form:  $HR = a_1 C_{norm}^{b_1}$ . We also tried a linear relationship (i.e.  $HR = a_1 + b_1 \times C_{norm}$ ) but the goodness of fit was worse in all diagrams. The model fitting was done taking account of the errors in both variables. The best fitting results are listed in Table 2. The best fitting  $b_1$  values in the  $HR2/C_{(3-5keV)_{norm}}$  diagrams are consistent with zero (contrary to the  $HR1/C_{(3-5keV+7-10keV)_{norm}}$  and  $HR3/C_{(3-5keV)_{norm}}$  diagrams). This result shows that the  $HR2$  variations are indeed independent of the source flux. The only exception is NGC 4051 which shows a  $HR2/C_{(3-5keV)_{norm}}$  slope which, although small, is significantly different from zero.

NGC 4051 also shows the largest absolute  $b_1$  values in all diagrams. The spectral variations in this source are thus a “steeper” function of the flux than in the other sources, i.e. for the same amplitude flux variations, the spectral variations in NGC 4051 are larger. Furthermore, the NGC 5506  $b_1$  value in the  $HR1/C_{(3-5keV+7-10keV)_{norm}}$  diagram is different from the values of NGC 5548 and MCG -6-30-15. This difference cannot be attributed to the

presence of a large absorbing column towards NGC 5506, unless the column density varies with the X-ray source flux. However such behavior has never been observed in S2 nuclei (Risaliti, Elvis and Nicastro 2001).

As Figures 4,5 and 6 show, a power law describes well the overall trend in all the color-flux plots. However, it does not give a statistically acceptable fit, except for the  $HR3/C_{(3-5keV)norm}$  diagrams (this is probably due to the larger errors associated with the HR3 values). There is significant scatter around the mean trends which shows that the spectra are significantly variable at any given “flux state” of the sources as well.

The spectral variability behavior of the sources could be studied with the frequently used color-color diagrams as well. For example,  $HR2$  vs  $HR1$  diagrams could be used to investigate, directly, whether the variations of the line’s  $EW$  are correlated with the primary spectrums slope changes. However, as we show in the Appendix, the fact that both  $HR1$  and  $HR2$  use the count rate in the  $[7 - 10]$  keV band, implies that there could exist misleading correlations in the  $HR2/HR1$  diagram. For that reason, we do not use any color-color diagrams to investigate the spectral variability behavior of the sources.

#### 4. Determination of spectral parameters from the hardness ratios

In order to understand the spectral variability behavior of the four sources in terms of commonly used spectral parameters, we used the widely used model consisting of a power law plus Fe line plus a reflection component. This model fits well the average X-ray/ $\gamma$ -ray spectrum of Seyfert 1 nuclei, especially in the 2–20 keV energy range (Nandra & Pounds 1994). We computed the model hardness ratios under different assumptions and compared them with the data as described in detail below. This comparison allows us to derive the main spectral characteristics (i.e. spectral index, reflection and iron line equivalent width) and to discuss the spectral variability exhibited by the different objects in our sample.

##### 4.1. The method

The model consists of a power law continuum of the form:  $f_E = NE^{-\Gamma}$ , where  $N$  is the normalization at 1 keV. We included a Compton reflection component using the PEXRAV model (Magdziarz & Zdziarski 1995) in XSPEC. This extra component calculates the X-ray spectrum when a source of X-rays is incident on optically thick, neutral (except hydrogen and helium) material. We fixed the inclination angle for the disk at  $i = 30^\circ$  (the shape of the reflection spectrum below 20 keV is relatively independent of the inclination angle). The iron

and light element abundances were kept fixed at the solar abundance values. The strength of the reflection component is governed by the parameter  $R$ , representing the strength of the reflected signal relative to the level of the incident power-law continuum. We also added a narrow Gaussian line ( $\sigma_{line} = 0.1$  keV) to simulate the iron line. The line energy was kept fixed at 6.4 keV so that the line is completely characterized by its equivalent width ( $EW$ ). Finally, except from NGC 5506, we do not consider the effects from neutral absorption in our calculations, since the absorbing column towards the direction of the sources is consistent with the Galactic value and does not affect the X-rays at energies  $> 2$  keV. For NGC 5506 we fix the value of  $N_H$  at  $3.6 \times 10^{22}$  cm $^{-2}$  (Perola 1998).

Assuming that this model gives a good representation of the spectral shape of the sources, we have a one-to-one correspondence between the data (the count rate in the four energy bands) and the model parameters ( $N$ ,  $\Gamma$ ,  $EW$  and  $R$ ). As a result, the observed count rates can be used to calculate the model parameters as described below.

Using XSPEC (v11.0), we computed the model count rate expected in different energy bands from the power law continuum, the reflection component and the Iron line for different values of the spectral index  $\Gamma$ , but fixing  $N = 1$ ,  $R = 1$ , and  $EW = 250$  eV ( $C_{E1-E2}^{pl}(\Gamma)$ ,  $C_{E1-E2}^R(\Gamma)$  and  $C_{E1-E2}^{Line}(\Gamma)$ , respectively, where  $(E1-E2) = [3-5], [5-7], [7-10]$  and  $[10-15]$  keV). Then, for each observation  $i$ , the observed count rate at each energy band is given by,

$$C_{E1-E2} = N_i \left[ C_{E1-E2}^{pl}(\Gamma_i) + R_i C_{E1-E2}^R(\Gamma_i) + \frac{EW_i}{250} C_{E1-E2}^{Line}(\Gamma_i) \right], \quad (1)$$

We have thus a system of four equations with four unknown variables ( $N_i$ ,  $\Gamma_i$ ,  $R_i$  and  $EW_i$ ) which is easily solvable for each pointing.

Since we are interested in the overall spectral behavior of the four sources during the total observational period, we did not solve the system of equations (1) for each observation. Instead, we used these equations to calculate the spectral slope and normalization at various flux states along the best fitting lines shown in Figure 3. Then we computed the  $HR2$  and  $HR3$  model ratios considering two different possibilities for the response of the reflecting material to the continuum variations: (a) The material responds with a short delay to the continuum variability, in which case the line's  $EW$  and the reflection component's parameter  $R$  should remain constant during the spectral variations. This is expected in the case when the material is located close to the X-ray source (i.e. the accretion disk). (b) The reflecting/reprocessing material does not respond simultaneously to the fast, intrinsic variations, as expected if the reprocessor is located away from the central source (i.e. the obscuring torus). In this case the line and the reflection component *flux* should remain constant.

The model  $HR2/C_{(3-5keV)norm}$  and  $HR3/C_{(3-5keV)norm}$  curves, in the case of constant  $EW$  and  $R$ , are plotted in Figures 4 and 5. In Figure 4, the dashed, dotted and dashed/dotted lines show the model curves in the case of constant  $EW = 0, 250$  and  $500$  eV respectively ( $R$  is kept constant to 1). The dashed, dotted and dashed/dotted lines in Figure 5 show the model curves in the case of constant  $R = 2, 1$  and  $0$  respectively.

To produce the model diagrams in the case of a remote reflector, we used the average  $HR$  values, listed in Table 1, to find the spectral parameters (i.e.,  $\Gamma$ ,  $N$ ,  $EW$  and  $R$ ) of the time average continuum of the four sources. Using XSPEC, we then deduced the flux of the line and of the reflection component in the average spectra. These fluxes were kept constant in order to estimate the model  $HR2$  and  $HR3$  values, at each  $C_{(3-5keV)norm}$ , using the respective  $(\Gamma, N)$  values (computed for  $R = 0$ ). The corresponding model curves are also plotted in Figures 4 and 5 (solid lines).

## 4.2. Results

### 4.2.1. The average spectra

Using equation (1) and the mean  $\bar{HR1}$ ,  $\bar{HR2}$  and  $\bar{HR3}$  values of each object, we estimated the mean spectral index  $\langle \Gamma \rangle$ , mean reflection normalization  $\langle R \rangle$  and mean iron line equivalent width  $\langle EW \rangle$ . The results are listed in Table 3. The values in this table show that NGC 4051 possesses the largest average  $R$  and  $EW$  values among the four sources. The mean spectral characteristics of the Seyfert 2 NGC 5506 are similar to those found for the two S1 objects, NGC 5548 and MCG -6-30-15.

Our results are in good agreement with the respective values that have been reported in the past, based on model fitting of the full band energy spectra. For example, Lamer et al. (2000, 2001), find an average value of  $\Gamma \sim 2.1$ ,  $R \sim 1.2$  and  $EW \sim 300$  eV for NGC 5506, and  $\Gamma \sim 2.05$ ,  $EW \sim 400$  eV for NGC 4051. These values are consistent with the values listed in Table 3 for the same objects. The average values for the line's  $EW$  that have been reported in the past for MCG -6-30-15 and NGC 5548 (Wang et al. 1999, Lee et al. 1999, and Chiang et al. 2000) are in agreement with the respective values in Table 3. The average  $R$  value that we find for MCG -6-30-15 also agrees with the values that Lee et al (1999) report, while it is slightly larger in the case on NGC 5548 (0.8 as opposed to  $\sim 0.5$  in Chiang et al 2000). Finally, the slope values that we find for MCG -6-30-15 and NGC 5548 are in good agreement with the values reported in the past for the same objects.

Interestingly, we find a correlation between  $\langle R \rangle$  and  $\langle \Gamma \rangle$  as well as a correlation between  $\langle EW \rangle$  and  $\langle \Gamma \rangle$ . When comparing the average spectra of the four sources, we see that the

sources which show harder spectra show smaller (average)  $R$  and  $EW$  values as well. This correlation is in agreement with the claims of Zdziarski et al. (1999).

#### 4.2.2. *The primary continuum variability*

The dashed lines in Figure 3 show the best fitting curves to the observed color-flux diagram of the four sources. On these lines, we have plotted the spectral slope values for a few normalized count rate values. These slope values are computed as explained in Section 4.1 in the case of  $R = 1$ . According to the model predictions, the observed  $HR1$  variations correspond to significant continuum slope changes. Differences in the spectral index up to a  $\Delta\Gamma \sim 0.3, \sim 0.2$  and  $\sim 0.2$  are necessary to explain the  $HR1$  variability in MCG -6-30-15, NGC 5506 and NGC 5548 respectively. In NGC 4051, differences larger than  $\Delta\Gamma \sim 1$  are needed to explain the observed  $HR1$  variations. Although we have excluded from our analysis the points that correspond to the “off-state” of this source, Uttley et al. (1999) have shown that the decline of the source towards this “off-state” is gradual. If the spectrum in this state is simply a reflection component produced by the torus and remains present at all times, then this is probably the dominant component in the X-ray spectrum of NGC 4051 in the observations that have the lowest count rate in Figure 3. As a result, the spectral slope that we measure could be affected by the shape of the reflection component, and the primary slope could be steeper than what we estimate. In fact, Lamer et al. (2001), find slope variations between  $\Gamma \sim 1.6$  and 2.3 when they subtract from the source’s spectra at the various flux states the “off-state” spectrum. As expected, their upper limit is consistent with ours ( $\sim 2.4$ , see Figure 3) while their lower limit is larger than ours.

In order to investigate further the effects of a constant flux reflection component on the spectral slope variability, we used the flux of the reflection component in the average spectrum of the sources (see Section 4.1) and assumed that it remains constant. In this case, since the reflection component contributes to the [7 – 10] keV band more than it does to the [3 – 5] keV band, it can result in an artificial flattening of the photon index, mainly when the source is at low flux states. For that reason, taking into account the constant reflection component flux at each energy band, we computed again the  $[N, \Gamma]$  values (using the best fitting line to the  $HR1$  vs flux plot, as explained in Section 4.1). Figure 6 shows again the plot of  $HR1$  as a function of the normalized  $([3 - 5] + [7 - 10])$  keV count rate, with the  $HR1$  values of NGC 4051 during the “low-state” included as well (in order to examine the intrinsic spectral slope values when the source is dominated by the reflection component). On the best fitting lines, we mark the new spectral slope values for a few normalized count rates, like we did in Figure 3.

As expected, due to the presence of a constant flux reflection component, smaller  $\Delta\Gamma$  variations are necessary in order to account for the observed  $HR1$  variations, and the “boundary”  $\Gamma$  values are now steeper. However, the differences between the results shown in Figures 3 and 6 are small. The assumption of a constant flux reflection component alone cannot account for the observed  $HR1$  variations. Intrinsic spectral slope variations of the order of  $\sim 0.2$  are still needed in order to explain the spectral variations in MCG -6-30-15, NGC 5506 and NGC 5548. Even in NGC 4051, intrinsic variations of  $\Gamma$  between  $\sim 1.5$  and  $\sim 2.4$  are still implied by the  $HR1$  variations. In fact, despite the presence of the constant flux reflection component, a primary component (albeit with a small normalization) with a very flat, variable slope needs to be present in order to account for the  $HR1$  values when the source is in the low/off-state.

More important effects on the implied  $\Gamma$  variations can have the variability behavior of the broad red wing of the Fe line in MCG -6-30-15. Based on *ASCA* observations, Iwasawa et al. (1996) found that the iron line in this source consists of a narrow core at an energy of  $\sim 6.4$  keV, and a broad wing extending to below 5 keV. While the narrow component cannot contribute significantly to the count rate in either the [3 – 5] or [7 – 10] keV band, the broad red wing will contribute to the observed [3 – 5] keV count rate. Iwasawa et al. (1996) found that the broad component can be fitted well with a Gaussian centered at 5.5 keV with a dispersion of 0.64 keV. They also found that the *EW* of this component component is variable, decreasing from  $\sim 600$  eV to  $\sim 100$  eV with increasing flux. Consequently, when the source is at low state, the broad wing can contribute significantly to the [3 – 5] keV band count rate, resulting in a flatter intrinsic slope.

In order to investigate this possibility, we recalculated the  $[N, \Gamma]$  values for MCG -6-30-15, assuming that the *EW* of the line’s red wing decreases from  $\sim 0.6$  keV to  $\sim 0.1$  keV, when the source is at the lowest/highest states in the present *RXTE* light curve. As expected, when the source is above its average flux state, the presence of the broad iron line wing does not affect significantly the estimation of the spectral slope value. However, as the flux decreases, the slope values that we estimate become flatter. At the lowest flux state (i.e. when  $C_{(3-5keV+7-10keV),norm} \sim 0.4$  in the MCG -6-30-15 plot of Figures 3, 6) we find a value of  $\Gamma \sim 1.7$ , as compared to  $\Gamma \sim 1.9$  that we find when we do not consider the effects of the line’s red wing. We conclude that, if the variability behavior of the extended red wing of the Fe line in MCG -6-30-15 on long time scales is similar to the behavior exhibited during the *ASCA* observations, the observed  $HR1$  variations of this source imply variations of the primary spectral slope of the order of  $\Delta\Gamma \sim 0.4 – 0.5$ .

Finally, using the  $[N, \Gamma]$  values at each flux state as shown in Figure 3, we computed the primary power law flux in the energy range between 1 – 300 keV. Figure 7 shows a plot

of this flux as function of the normalized source count rate. In NGC 4051, we find that the luminosity variations have an amplitude much smaller than that of the observed flux variations. In this source, the large amplitude [3 – 15] keV flux variations appear to be caused mainly by the large amplitude continuum slope variations. In the other sources, the peak to peak amplitude of the luminosity change is  $\sim 2$ . This is smaller but comparable with the amplitude of the observed flux variations. However, since the variability behavior of the high energy cut-off component cannot be studied with the present *RXTE* data, it is possible that the amplitude of the luminosity variations is smaller in reality if there are significant cut off variations. In fact, Petrucci et al. (2000) find that in NGC 5548 (the source that shows the largest amplitude luminosity variations in Figure 7) the cut-off variations are associated with the spectral slope variations in such a way so that the total X-ray luminosity remained constant during the long *Beppo SAX* observation.

#### 4.2.3. The line variability

Filled squares in Figure 4 show the average  $HR2$  values over various flux (i.e.  $C_{(3-5keV)_{norm}}$ ) bins. The size of the bins was variable so that 15 points were included in each one. These points indicate the average  $HR2$  behavior as a function of the soft band flux and are close to the best fitting lines of the  $HR2/C_{(3-5keV)_{norm}}$  diagrams.

The “constant  $EW$ ” model predictions do not agree well with the average  $HR2$  values. Instead, the model curves suggest rather complex variations for the line’s  $EW$  in all sources. It appears that, on average, the line’s  $EW$  decreases as the source flux increases. For example, for NGC 5548, when the source is at the lowest flux state the line’s  $EW$  is  $\sim 250$  eV. As the source flux increases, the line’s  $EW$  decreases to  $\sim 50$  eV. In NGC 4051, when the normalized soft band count rate is below  $\sim 0.7$ , the line’s  $EW$  appears to increase strongly, reaching a value larger than 500 eV at the very low flux states. The tendency of the line’s  $EW$  to decrease with increasing source flux also appears in the color-flux diagrams of NGC 5506 and MCG -6-30-15 but the amplitude of the  $EW$  variations is smaller in these two sources.

In the same Figure, we have also plotted the “constant line flux” model curves. In this case, the model predictions are consistent with the average  $HR2$  values, except perhaps NGC 5506 where the model curve lies above the average  $HR2$  values. We can get an agreement between the model predictions and the NGC 5506 data if we increase slightly the flux of the line that we add to all the model spectra.

Column 2 and 3 in Table 4 lists the slope of the model curves shown in Figure 4. The

$b_{CEW}$  values correspond to the slope of the model curves under the assumption of constant line’s  $EW$ , while  $b_{CLF}$  is the slope of the constant line flux model curves. Comparison of these values with the best fitting slope values listed in Table 2, shows clearly that the constant flux model predictions agree better with the data; their slopes are consistent with the best fitting slope values. On the other hand, the difference between the constant  $EW$  model curve slopes and the best fitting slopes is larger than  $3\sigma$  in all sources.

#### 4.2.4. The reflection component variations

As before with Figure 4, filled squares in Figure 5 show the average  $HR3$  values as a function of the soft band flux. In the same Figure, we also show both the “constant  $R$ ” and “constant reflection flux” model curves.

Due to the large scatter in the  $HR3/C_{(3-5keV)_{norm}}$  diagrams of all sources, and the similarity of the model curves under the two different assumptions, it is not clear which model curves fit better the data. In the MCG -6-30-15 and NGC 5506 plots, comparison between the constant  $R$  model curves and the average  $HR3$  values show that  $R$  slightly decreases with increasing source flux, in agreement with the  $EW$  dependency on the flux in these sources. However, most of the average  $HR3$  points are close to the constant  $R = 1$  model curve, and only the lowest flux  $HR3$  value is clearly closer to the constant  $R = 2$  curve. In NGC 5548,  $R$  appears to remain constant during the spectral variations at a value smaller than 1. Similarly, in NGC 4051, the average  $HR3$  values imply spectral variations under constant  $R$  (with a value between 1 and 2). Only the lowest flux points suggest a decreasing  $R$  value with decreasing source flux. However, this is again caused by the fact that the spectral slope that we measure from observations with the lowest flux represents the shape of the reflection component itself. Hence the  $\Gamma$  values are larger and the  $R$  values are smaller than in reality (see discussion in section 4.2.1)

The constant reflection flux model curves also provide a good fit to the average  $HR3$  values in all sources. Columns 4 and 5 in Table 4 list the slopes of the constant  $R$  and constant reflection flux model curves ( $b_{CR}$  and  $b_{CRF}$  respectively). Comparison between these values and the best fitting slopes of the  $HR3/C_{(3-5keV)_{norm}}$  diagrams (listed in table 2) shows that all model curves are consistent with the data. The only exception is the  $b_{CR}$  value of NGC 5506, which show a  $5\sigma$  difference with the best fitting slope.

## 5. Comparison with previous studies

The spectral variability properties of the four sources that we study in the present work have already been addressed previously. In most cases, the results are based on spectral fitting of the power law plus reflection model to the observed energy spectra.

All studies have shown that as the source brightens the continuum spectrum steepens. Differences in the spectral slope up to  $\Delta\Gamma \sim 0.3, 0.2$  and  $0.15$  have been observed in MCG -6-30-15 (Lee et al. 1999), in NGC 5506 (Lamer et al. 2000) and in NGC 5548 (Chiang et al. 2000; Petrucci et al. 2000). Our results are consistent with the previous studies. We find that the observed  $HR1$  variations correspond to larger spectral slope changes. This is because we have detected flux variations of a larger amplitude. In the case of NGC 4051 we find a larger  $\Delta\Gamma$  variations compared to Lamer et al. (2001), but as we discussed in section 4.2.1, this is due to the significant contribution of the “off-state” spectrum to the source’s spectra at low flux states.

Variability of the iron line’s  $EW$  and of the reflection fraction  $R$  have also been observed. Using ASCA data of 39 AGNs, Nandra et al. (1997) found a clear decrease in the iron line’s  $EW$  with increasing source luminosity. Lee et al. (2000), Lamer et al. (2000) and Chiang et al. (2000) also find that the iron line’s  $EW$  decreases with increasing source flux in MCG -6-30-15, NGC 5506 and NGC 5548 respectively. These results are consistent with ours. Furthermore, the dependence of the combined “narrow” and “disk” line’s  $EW$  on the source’s flux level that Lamer et al. (2001) find in NGC 4051 is entirely consistent with our results shown in Figure 4. On the other hand, Wang et al. (1999) have observed a positive correlation between the line’s  $EW$  and the source flux in NGC 4051 using ASCA data, contrary to our results. We note however that NGC 4051 was “weakly” variable (factor of 2) during the ASCA pointing in comparison to variations of more than a factor 10 in our case. Furthermore our  $HR2/C_{(3-5keV)_{norm}}$  diagram for this object shows large scatter around the mean trend. We thus believe that the results of Wang et al. (1999) are consistent with our conclusions.

Lamer et al. (2000) find that the reflection fraction in NGC 5506 decreases with source flux; in particular it is not correlated to the continuum slope as derived from direct fitting of *RXTE* spectra. Chiang et al. (2000) find that the reflection fraction remains constant in NGC 5548. These results are also consistent with ours. On the other hand, Lee et al (2000) find that the reflection fraction in MCG -6-30-15 increases with source flux (and is anticorrelated with the line’s  $EW$ ) contrary to what we obtain. Finally, in NGC 4051, Lamer et al. (2001) find that the reflection fraction of the “disk component” (i.e. the primary spectrum without the contribution of the “off-state” spectrum) is very small. Therefore if the only reflection component is the one that is observed in the “off-state” then its flux should

remain constant. As Figure 5 shows, our results are entirely consistent with this possibility.

## 6. Discussion

We have studied in detail the spectral variability of four Seyfert galaxies (NGC 4051, MCG -6-30-15, NGC 5506 and NGC 5548) over a  $\sim 3$  years period. Using *RXTE* data we computed hardness ratios which are sensitive to the primary slope, iron line and reflection component variations ( $HR1$ ,  $HR2$  and  $HR3$  respectively). Our results show that all the sources exhibit significant spectral variability. We find that  $HR1$  and  $HR3$  decrease as the source flux increases while the  $HR2$  variations are independent of the source flux. The spectral variability behavior of the Narrow Line Seyfert 1 galaxy NGC 4051 and the Seyfert 2 galaxy NGC 5506 is similar to the behavior of MCG -6-30-15 and NGC 5548, the two Seyfert 1 nuclei in our sample. There are also minor differences. NGC 4051 in particular shows the largest spectral slope variability amplitude among the four sources.

Our approach to study the spectral variability of the sources is different from previous studies. Instead of a detailed spectral study that uses the full energy spectrum (usually in the  $\sim 2 - 15$  keV band with *RXTE* data) at a few epochs (at best), we use a large number of short exposures over a long period, and compare the observed color-flux diagrams with the predictions of the simple “power law plus Compton reflection component plus iron line” model. The hardness ratios cannot be used in order to investigate whether the model can fit well the X-ray spectrum of the sources or not, however, it is known from past studies that this model does provide a good representation of the X-ray energy spectra of AGN. In this case, due to the large number of observations which are regularly distributed over a long period (much longer than the typical duration of the AGN observations) the hardness ratios can be used to investigate, accurately, which components in the X-ray spectra of AGN are responsible for the correlations that we find in the color-flux diagrams.

We did this by constructing various model color-flux curves. For the  $HR2/C_{(3-5kev)norm}$  and  $HR3/C_{(3-5kev)norm}$  model curves we considered two possibilities for the reflecting and the line producing material. First, we produced model curves assuming that the material responds fast to the continuum variations. In this case the line’s  $EW$  and the reflection parameter  $R$  remain constant during the spectral slope variations. Alternatively, in the case when the material does not respond quickly to the continuum variations, it is the flux of the line and the reflection component that remains constant.

Our main results from the comparison of the observed color-flux plots with the predictions of the “power law + reflection + iron line” model are the following:

- 1) The primary continuum slope is variable. Averaging HR1 in fixed flux intervals, the derived slope is positively correlated with the soft band flux. At each flux state, there are also significant slope variations around the mean slope that corresponds to that state.
- 2) As the soft band flux increases, the line's  $EW$  decreases (Figure 4). There is an indication that the reflection parameter  $R$  also decreases with increasing flux in the case of NGC 5506 and MCG -6-30-15 (Figure 5). In NGC 4051 and NGC 5548,  $R$  remains constant during the primary spectral and flux variations. In any case, the  $HR3$  color-flux diagrams do not show any increase of  $R$  with increasing source flux (i.e. as the primary spectrum steepens).

### 6.1. Power-law slope variability

Spectral slope variability is predicted by thermal Comptonization models. An increase of the soft input photon flux will result in a reduction of the corona temperature, a steepening of the intrinsic spectrum and hence an increase in the soft X-ray band flux. This response of the X-ray spectrum to the soft input photon changes has already been observed in NGC 7469 (Nandra et al. 2000) and NGC 5548 (Petruzzi et al. 2000). In the simplest case, we expect a correlation between the spectral slope and the soft band flux, as observed in Figure 3. It is remarkable how similar the average spectral behavior is for three of the sources and for all the intensity states covered. In particular 5506, a Seyfert 2, follows the same behavior as 5548 and MCG -6-30-15.

The fact that the spectral slope variations of NGC 4051 have a larger amplitude could be due in part to a larger variation of the strong soft component known to be present in this source, affecting mainly the [3 – 5] keV band, hence resulting in a steeper spectrum. As we already discussed in Section (4.2.1), the very flat spectra that we observe at the lowest flux states could be the result of the fact that in these cases the reflection component is prominent in the energy spectrum (affecting mainly the [7 – 10] keV band) so that the estimated slope determines mainly the shape of this component instead of the primary continuum.

Apart from the average trend, the  $HR1$ –flux plots also show significant scatter around the best fitting lines. Therefore, spectral slope variations happen at constant flux as well. Since different slope values result in the same soft band flux, these variations should be associated with luminosity changes. Apart from variability induced by the Compton-cooling process, other processes that affect the corona properties (like and the corona heating process for example) should also be variable.

## 6.2. Iron line and reflection component variability

In NGC 5506 and MCG -6-30-15, the line's  $EW$  and the reflection parameter  $R$  vary proportional to each other (i.e. in the same way with the source flux). This implies that the material which emits the iron line is also responsible for the reflection hump. In the other two sources,  $R$  remains constant while  $EW$  decreases with the source flux. If this is the case, the line emitting and reflecting material should not be the same. However, it would be difficult to explain why matter that produces the iron line cannot produce the reflection hump as well (and vice versa).

Changes in the line's  $EW$  and the reflection parameter  $R$  could be the result of variations in the geometry of the system. For example, if the solid angle subtended by the reflector decreases, both the line's  $EW$  and the reflection parameter should also decrease. A relativistic outflow of the X-ray source could produce such an effect. However, at the same time, it should also be able to produce a softening of the primary spectrum and an increase in the total X-ray luminosity in order to explain the simultaneous increase of the soft band flux as both  $EW$  and  $R$  decrease.

The observed  $EW$  and  $R$  variability behavior of the sources can be explained in a consistent way if the reprocessing material does not respond instantly to the continuum spectral variations. As the solid lines in Figures 4 and 5 show, the assumption of constant flux for the line and the reflection component during the spectral variations can account for the mean trends in the  $HR2$  and  $HR3$  color-flux diagrams. As the source luminosity and hence the continuum normalization increases, the soft band flux increases (see Figure 7) while both  $EW$  and  $R$  decrease because the flux of the line and reflection component remain constant. Since the average spectral properties of the sources are not identical (see Table 3), the constant flux model curves can explain quite well the spectral variations although the best fitting lines in the color-flux plots are not the same for all sources. Even in the cases where  $R$  remains constant during the flux variations (e.g. NGC 5548) the model curves can still fit well the color-flux diagrams. The reason is that the constant flux and constant  $R$  model curves are quite similar; we need data with smaller uncertainty to discriminate between the two cases.

A natural explanation for the fact that the reprocessor does not respond to the fast intrinsic variations is that it is located away from the central source, i.e. it is associated with the obscuring torus in the objects. Interestingly, this possibility, at least in the case of NGC 5548, is supported by a recent *CHANDRA* observation of this source which has revealed the existence of a narrow Fe K emission with a center energy of  $\sim 6.40$  keV and  $EW \sim 130$  eV (Yaqoob et al. 2001), similar to the average line's  $EW$  we find for this object (Table 3). As these authors comment, the line should be produced in material that is

located away from the central source, in agreement with our results from the hardness ratios variations.

Our results do not exclude reprocessing from material close to the central source (i.e. from the accretion disk). The *HR2* color-flux diagram shows significant scatter around the best fitting lines. These variations could be the result of the slope variations that cause the scatter in the *HR1* color-flux plot (the [7 – 10] keV band count rate contributes to both the *HR1* and *HR2* ratios). However, the *HR2* variations at constant flux could also be the result of fast variations of the iron line flux.

Finally, we find a correlation between the spectral parameters of the average spectra of the individual sources in the sense that softer spectra show a larger reflection component  $R$  and line's  $EW$  value. This is similar to the correlation between  $R$  and  $\Gamma$  of Zdziarski et al. (1999) for different sources. However, we do not find the same correlation between  $R$  and  $\Gamma$  during the spectral variations within each source. Our results show clearly that the reflection parameter  $R$  is not increasing with increasing source flux (i.e. as the spectrum softens). The  $R$ -flux correlation that we find is opposite to what we would expect if  $R$  was decreasing with decreasing  $\Gamma$ . Therefore, we do not confirm the Zdziarski et al. (1999) correlation between  $\Gamma - R$  during the spectral variations within each source. If the bulk of reprocessing originates from neutral material located away from the central source *and* the  $\Gamma - R$  relationship is valid for different sources, then its origin is not obvious. It probably depends on a physical parameter that varies from one object to the other, like black hole mass or luminosity (which depends on the accretion rate as well). For example, in the more luminous sources the flux of the soft photons could be stronger resulting in a stronger cooling of the plasma hence a softer spectrum. At the same time, the effective solid angle subtended by the reflector should also be larger, either because the reflector is located closer to the central source (which seems unlikely), or because the reflector is having a larger size.

## 7. Conclusions

We have used monitoring *RXTE* light curves to study the spectral variability in four Seyfert galaxies, namely NGC 4051, MCG -6-30-15, NGC 5506 and NGC 5548. The large number of observations over a long period (over  $\sim 3$  years) allowed us to study their overall spectral variability behavior over many, different flux states. This is not possible to achieve with the normal observations of AGN which last typically less than a few days.

The exposure time of each observation is not long enough to perform model fitting to the [3 – 15] keV band energy spectrum of the sources, but adequate to give us accurate

measurements of the flux in different energy bands. For that reason, we computed hardness ratios, we produced color-flux diagrams and we used the commonly used “power law plus reflection plus iron line” model to interpret our results.

All sources show similar spectral variations. The variations in the *HR1* color-flux plot imply primary slope changes which affect significantly the soft band flux. The mean trends in the *HR2* and *HR3* color plots can be explained if we assume that the flux of the line and of the reflection component remains roughly constant during the underlying continuum variations. A constant line and reflection component flux is naturally expected if the reprocessing material is located away from the central source. The fact that the model under the assumption of constant line and reflection flux describes well the mean trend in the color-flux of all sources suggests that they operate in the same way. What are different is the amplitude of the slope variations (NGC 4051 shows the largest amplitude slope variability) and the average spectrum of each source. Interestingly, we find that sources with softer energy spectra show larger *EW* and *R* values as well. However, within each source, we find the opposite behavior. The reflection parameter *R* and the line’s *EW* decrease (instead of increasing) with increasing source flux (and hence softening of the energy spectrum). Therefore, we confirm the *R* –  $\Gamma$  relationship of Zdziarski et al. (1999) for the average spectra of the sources, but not for the spectral variations within each source.

The significant scatter around the best fitting lines in the *HR1* and *HR2* color-flux diagrams shows that the spectral variability in AGN is more complicated than the mean trends of the color-flux plots suggest. The low amplitude slope variations at constant flux imply that Compton-cooling is not the only process that determines the properties of the active corona. The *HR2* variations around the mean trend could imply low amplitude, line flux variations. If true, they could be the result of reprocessing from material near the central source.

We thank the *RXTE* team for their operation of the satellite. IEP thanks the Osservatorio Astronomico di Brera for hospitality. We also thank an anonymous referee for making helpful suggestions. Part of this work was done in the TMR research network ‘Accretion onto black holes, compact stars and protostars’ funded by the European Commission under contract number ERBFMRX-CT98-0195.

## APPENDIX

### FALSE CORRELATIONS IN THE COLOR-COLOR PLOTS

As stated in the main text, the use of the same count rate in the determination of two colors can introduce misleading correlations in the color-color diagrams. To illustrate

this, in the top plot in Figure 8 we have plotted the  $HR2$  versus  $HR1$  colors in the case of MCG -6-30-15. There appears to exist a strong correlation between the two ratios in the sense that  $HR2$  increases with increasing  $HR1$ . The solid line in this plot shows the best fitting line to the color-color diagram (we find a best fitting slope of  $1.24 \pm 0.09$ ). This is not consistent with the  $HR2$  vs  $C_{(3-5keV)_{norm}}$  color-flux diagram of the same source which showed that  $HR2$  remains constant, independent of the source flux state. Since the spectral slope is correlated with the source flux, we did not expect to see a correlation between  $HR2$  and  $HR1$  either.

We performed a numerical experiment to verify whether the observed correlation between  $HR2$  and  $HR1$  is an artifact, caused by the inter-dependence of the two variables. First, we assumed 124 points (equal to the number of points in the MCG -6-30-15 light curve) evenly distributed in the interval between 0.4 and 1.8 (i.e. the limits of the  $C_{(3-5keV)_{norm}}$  values of MCG -6-30-15). Using the best fitting power law model line of the  $HR1$  vs  $C_{(3-5keV)_{norm}}$  color-flux diagram, we computed the  $HR1$  values that correspond to these values, and hence the respective  $[7 - 10]$  keV band count rate. To compute the  $C_{5-7keV}$  keV values, we used the  $C_{7-10keV}$  values and assumed a constant  $HR2$  value (equal to the mean  $HR2$  value listed in Table 1) at each flux state. Then we added appropriate random Gaussian “errors” to the simulated  $C_{3-5keV}$ ,  $C_{5-7keV}$  and  $C_{7-10keV}$  points and computed the  $HR1$  and  $HR2$  colors using the randomized simulated count rates.

The simulated  $HR1$  and  $HR2$  vs.  $C_{(3-5keV)_{norm}}$  color-flux diagrams are shown in Figure 8 (second and third plot from top). They are similar to the respective diagrams in Figures 3 and 4. The bottom plot in Figure 8 shows the  $HR2$  vs  $HR1$  diagram using the simulated colors. Despite the fact that we had computed the  $C_{5-7keV}$  simulated values in such a way so that  $HR2$  would remain constant at the same value irrespective of the source flux or spectral state, the simulated color-color plot shows a strong correlation between  $HR2$  and  $HR1$ , as if larger values of  $HR2$  correspond to larger values of  $HR1$  as well. In fact, the slope of the best fitting line to the simulated color-color plot (shown with a solid line in Figure 8) is  $1.49 \pm 0.17$ . The difference between this value and the best fitting slope value of the observed color-color diagram is  $0.25 \pm 0.17$ . This result shows that purely statistical effects are highly likely to reproduce the observed correlation between  $HR1$  and  $HR2$ . Since both ratios use  $C_{7-10keV}$  in the numerator, when  $C_{7-10keV}$  is higher than average due to a statistical fluctuation, then both  $HR1$  and  $HR2$  will be higher on average, resulting in an almost one-to-one correlation between them.

## REFERENCES

Antonucci, R. 1993, *ARA&A*, 31, 473

Chiang, J, Reynolds, C.S., Blaes, O.M., Nowak, M.A., Murray, N., Madejski, G., Marshall, H.L., & Magdziarz, P. 2000, *ApJ*, 528, 292

Ghisellini, G., Haardt, F., & Matt, G. 1994, *MNRAS*, 267, 743

Gondek, D., Zdziarski, A.A., Johnson, W.N., George, I.M., McNaron-Brown, K., Magdziarz, P., Smith, D., & Gruber, D.E. 1996, *MNRAS*, 282, 646

Guainazzi, M. et al. 1998, *MNRAS*, 301, L1

Haardt, F., & Maraschi, L. 1991, *ApJ*, 380, L51

Haardt, F., & Maraschi, L. 1993, *ApJ*, 413, 507

Iwasawa, K., et al. 1996, *MNRAS*, 282, 1038

Lamer, G., Uttley, P., & McHardy, I.M. 2000, *MNRAS*, 319, 949

Lamer, G., Uttley, P., McHardy, I.M., & Jahoda, K. 2001, *MNRAS*, submitted

Leighly, K.M 1999a, *ApJS*, 125, 297

Leighly, K.M 1999b, *ApJS*, 125, 317

Lee, J.C., Fabian, A.C., Brandt, W.N., Reynolds, C.S., & Iwasawa, K. 1999, *MNRAS*, 310, 973

Magdziarz, P. & Zdziarski, A. A 1995, *MNRAS*, 273, 837

Nandra, K., & Pounds, K. A. 1994, *MNRAS*, 268, 405

Nandra, K., George, I.M., Mushotzky, R.F., Turner, T.J., & Yaqoob, T. 1997, *ApJ*, 488, L91

Nandra, K., Le, T., George, I.M., Edelson, R.A., Mushotzky, R.F., Peterson, B.M., & Turner, T.J. 2000, *ApJ*, 544, 734

Perola, G.C. 1998, *Nuclear Physics B (Proc. Suppl.)*, 69/1-3, 477

Petrucci, P.O., Haardt, F., Maraschi, L., Grandi, P., Matt, G., Nicastro, F., Piro, L., Perola, G. C., & De Rosa, A. 2000, *ApJ*, 540, 131

Risaliti, G., Elvis, M., & Nicastro, F. 2001, *ApJ*, in press

Uttley, McHardy, I.M., & Papadakis, I.E. 2002, *MNRAS*, in press

Uttley, P., McHardy, I.M., Papadakis, I.E., Guainazzi, M., & Fruscione, A. 1999, *MNRAS*, 307, L6

Wang, J.X., Zhou, Y.Y., Xu, H.G., & Wang, T.G. 1999, *ApJ*, 516, L65

Yaqoob, T., George, I.M., Nandra, K., Turner, T.J., Serlemitsos, P.J., & Mushotzky, R.F.  
2001, *ApJ*, 546, 759

Zdziarski, A. A, Lubinski, P., & Smith, D. A. 1999, *MNRAS*, 303, L11

Fig. 1.— The *RXTE* 2 – 10 keV monitoring light curves of NGC 4051, MCG -6-30-15, NGC 5506 and NGC 5548. The light curves are normalized to their weighted mean. The time axis is on days since the first observation of each source. Note the different sampling scheme throughout the observing period. Errors are included in the plotted points but are too small to be seen.

Fig. 2.— The hardness ratio light curves for the four sources. The solid lines show the mean value of each light curve. Time is measured (in days) since first observation of each source. Note the different  $y$ –axis scaling in the case of NGC 4051.

Fig. 3.— The  $HR1$  values plotted as a function of the normalized  $[3-5] + [7-10]$  keV source count rate. The dashed lines show the best fitting power law to the data. Filled squares show the slope of a power law plus reflection model that corresponds to the respective [flux,  $HR1$ ] values. These slope values were computed as described in Section 4.1

Fig. 4.— The  $HR2$  values plotted as a function of the normalized  $[3-5]$  keV source count rate. Filled squares show the average  $HR2$  values in various flux bins. In all plots, the dashed, dotted and dashed-dotted lines show the color-flux model curves in the case of a power law plus reflection plus iron line with constant  $EW = 0, 250$  and  $500$  eV respectively. Solid lines show the model color-flux curves in the case of a constant flux line. The model curves were computed as explained in Section 4.1

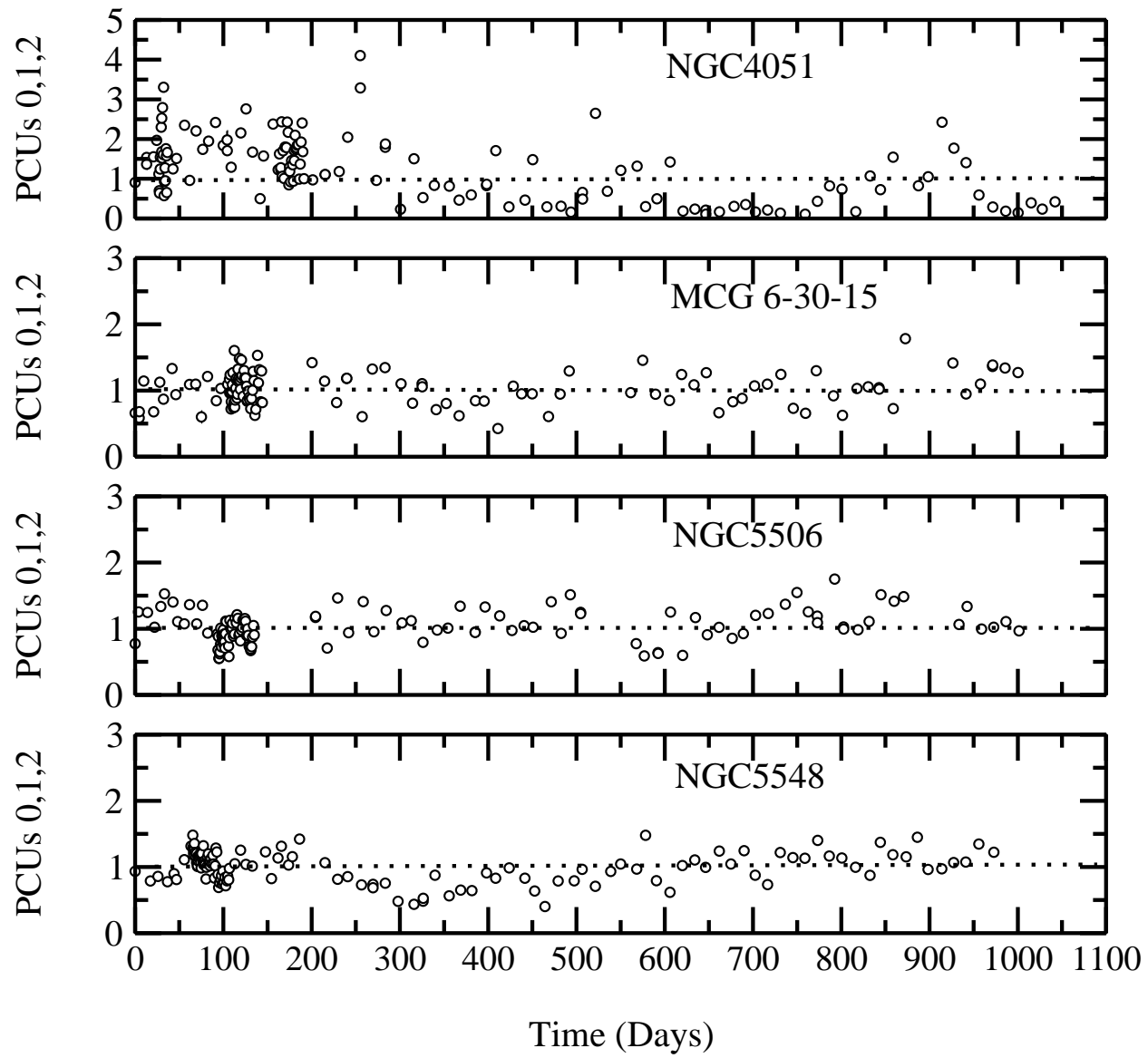
Fig. 5.— The  $HR3$  values plotted as a function of the normalized  $[3-5]$  keV source count rate. Filled squares show the average  $HR3$  values in various flux bins. In all plots, the dashed, dotted and dashed-dotted lines show the color-flux model curves in the case a power law plus reflection with constant  $R = 2, 1$  and  $0$  respectively. Solid lines show the model color-flux curves in the case of a constant flux reflection. The model curves were computed as explained in Section 4.1

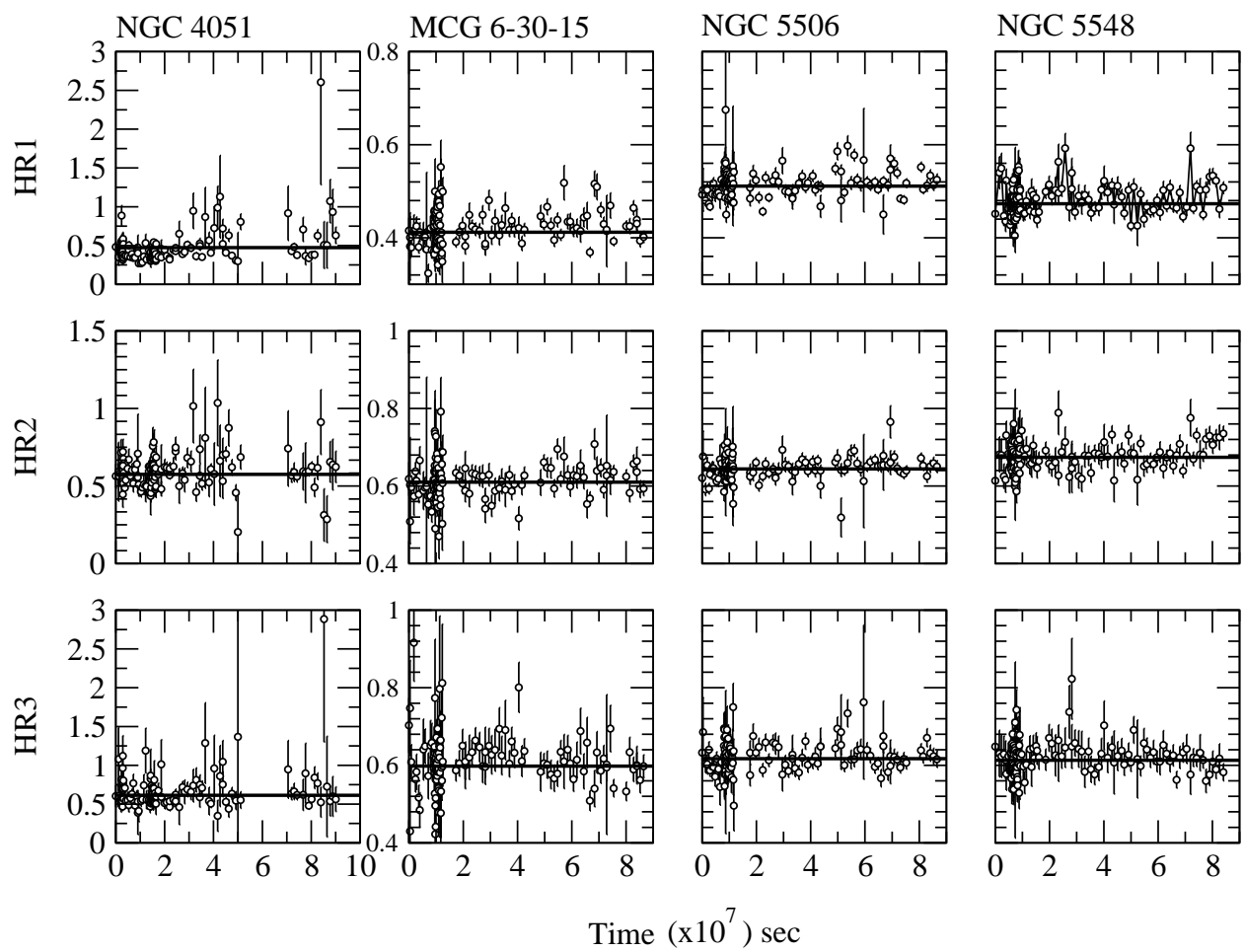
Fig. 6.— The  $HR1$  values plotted as a function of the normalized  $[3-5] + [7-10]$  keV source count rate. As in Figure 3, the dashed lines show the best fitting power law to the data. Filled squares show the slope of the power law that corresponds to the respective [flux,  $HR1$ ] values in the case when there exists a reflection component whose flux remains constant. These values were computed as described in Section 4.2.2. Note that, in this Figure, we have included the data from the low state of NGC 4051.

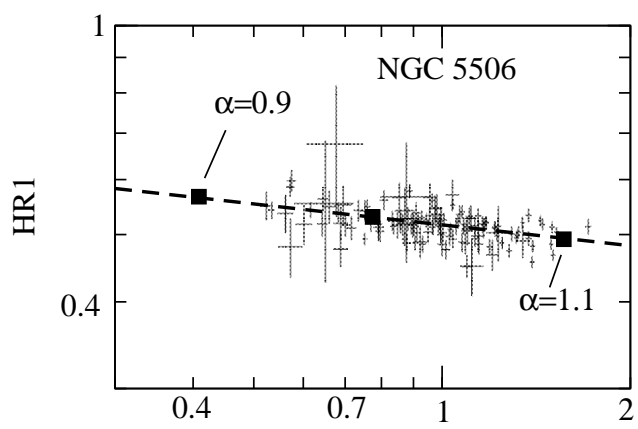
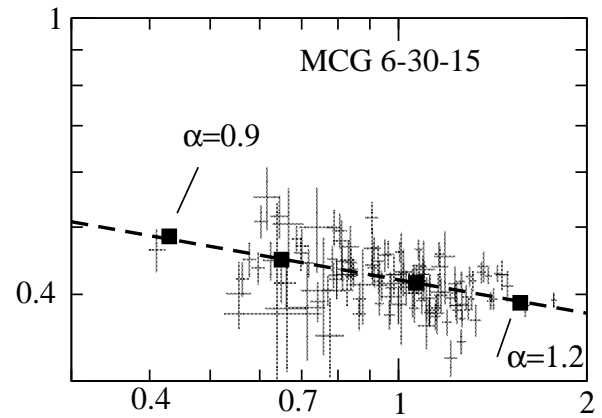
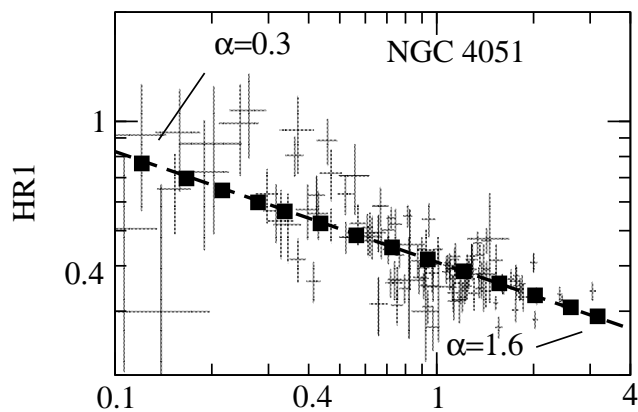
Fig. 7.— Plot of the model,  $[1-300]$  keV flux as a function of the normalized, soft band count rate. The peak-to-peak variation in the source luminosity is less than  $\sim 2$  in all cases.

Fig. 8.— Plot of the  $HR2$  vs  $HR1$  color-color diagram in the case of MCG -6-30-15 (a). A

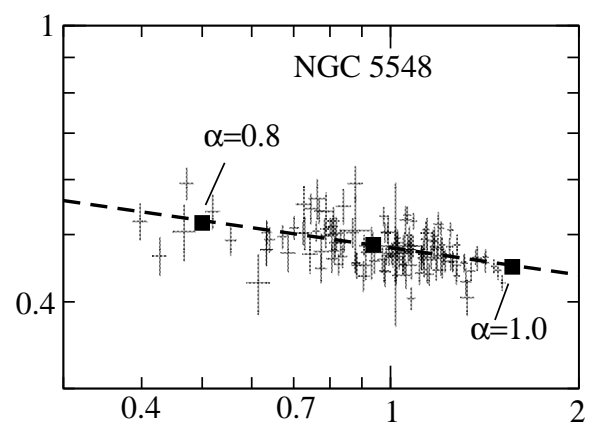
strong correlation is observed. The solid line shows the best fitting line to the data. The panels (b) and (c) show a plot of the  $HR1$  and  $HR2$  vs normalized [3 – 5] keV count rate color-flux diagrams for a set of simulated light curves (see Appendix). Panel (d) shows the  $HR2$  vs  $HR1$  color-color diagram for the same set of simulated light curves. Although the light curves were constructed in such a way so that  $HR2$  is constant, there exists a strong correlation between  $HR2$  and  $HR1$  (similar to the correlation between the observed  $HR1$  and  $HR2$  values of MCG -6-30-15 shown in panel (a)). This correlation is caused by random, statistical effects.



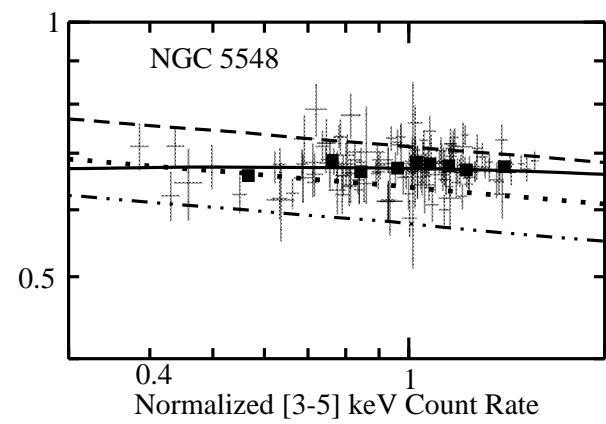
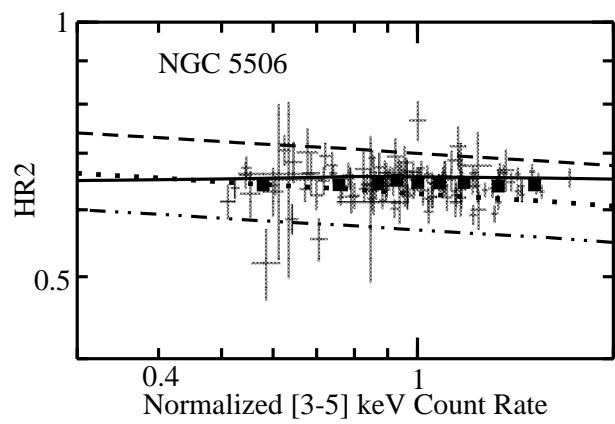
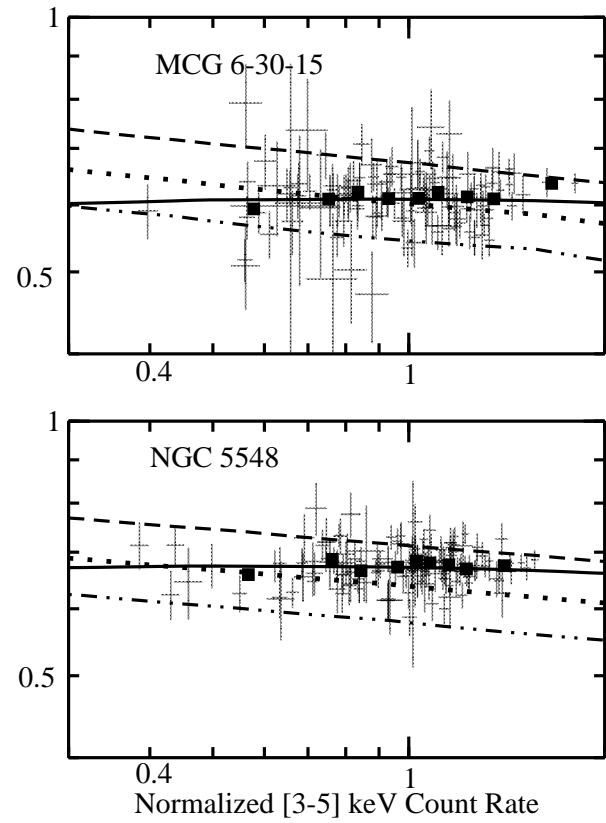
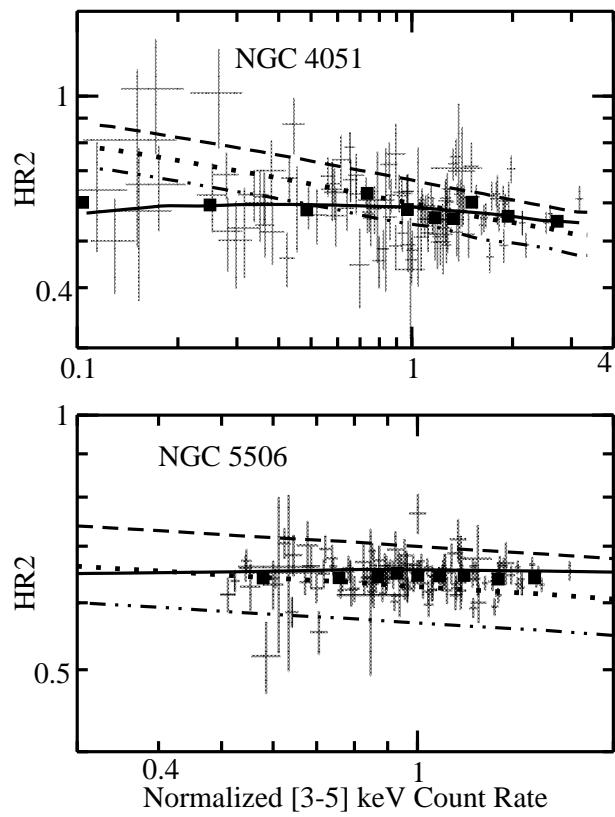


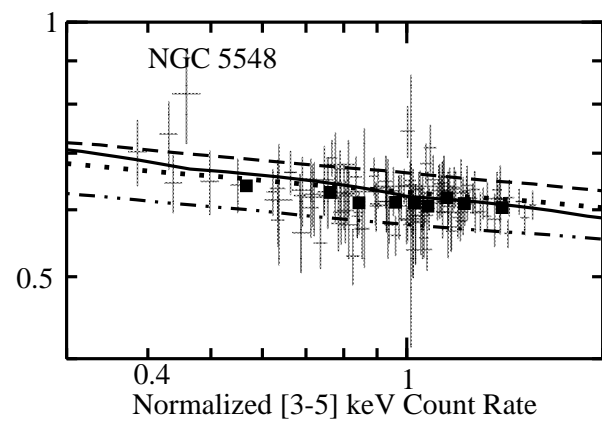
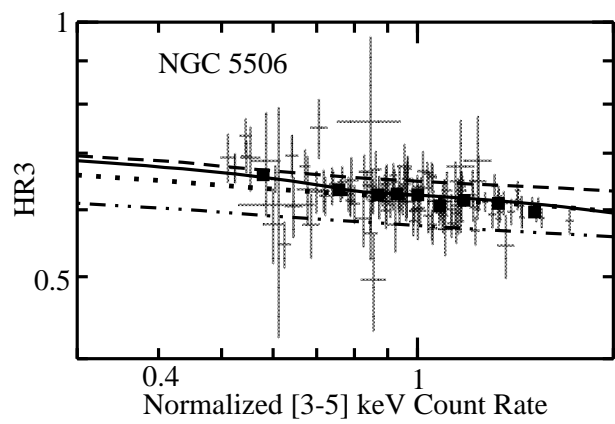
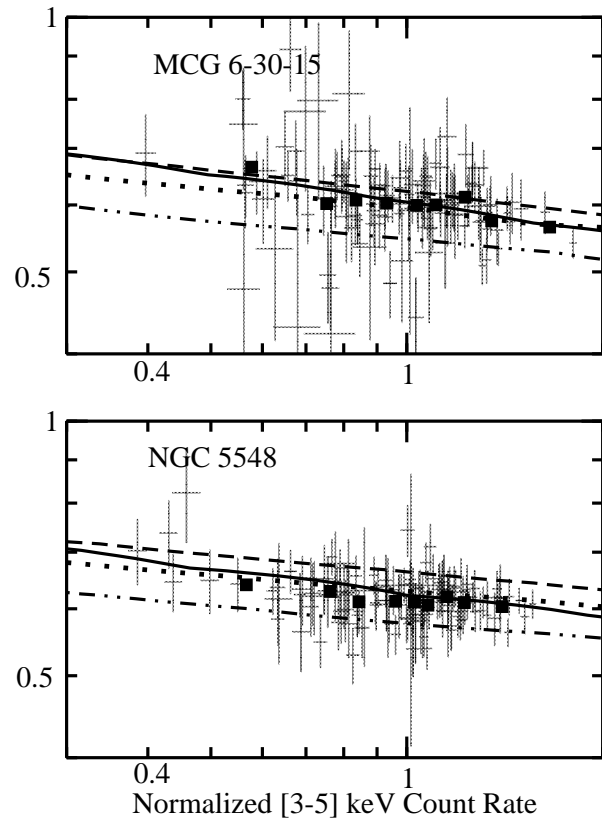
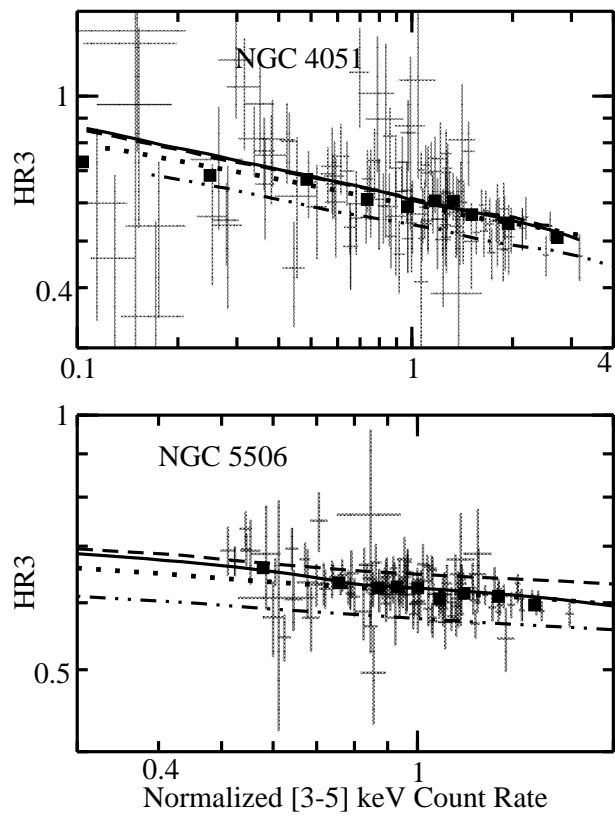


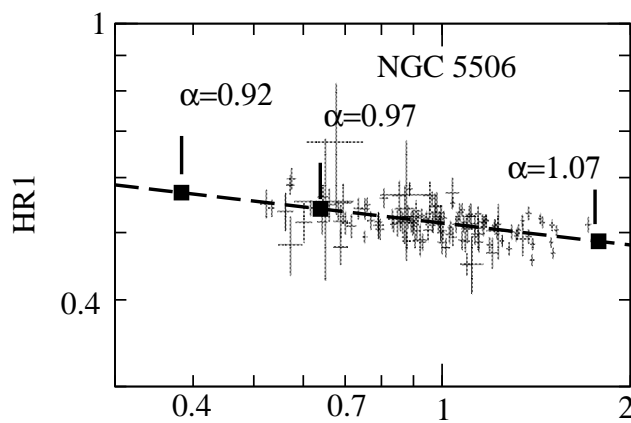
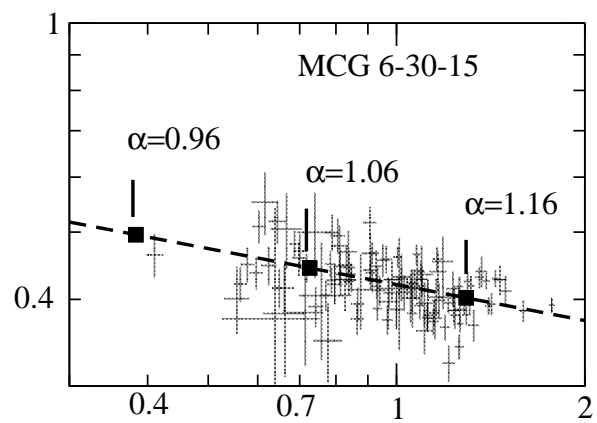
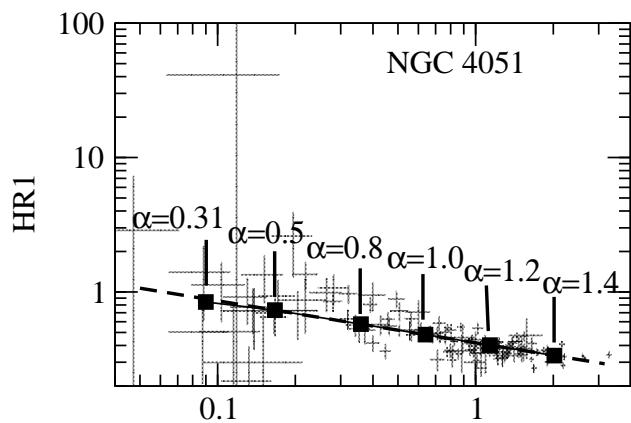
Normalized [3-5]+[7-10] keV CR



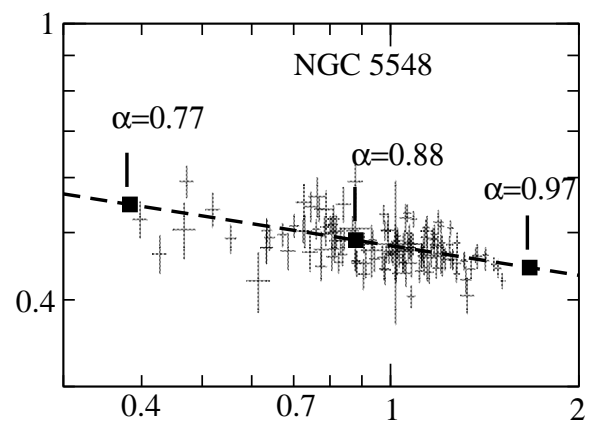
Normalized [3-5]+[7-10] keV CR



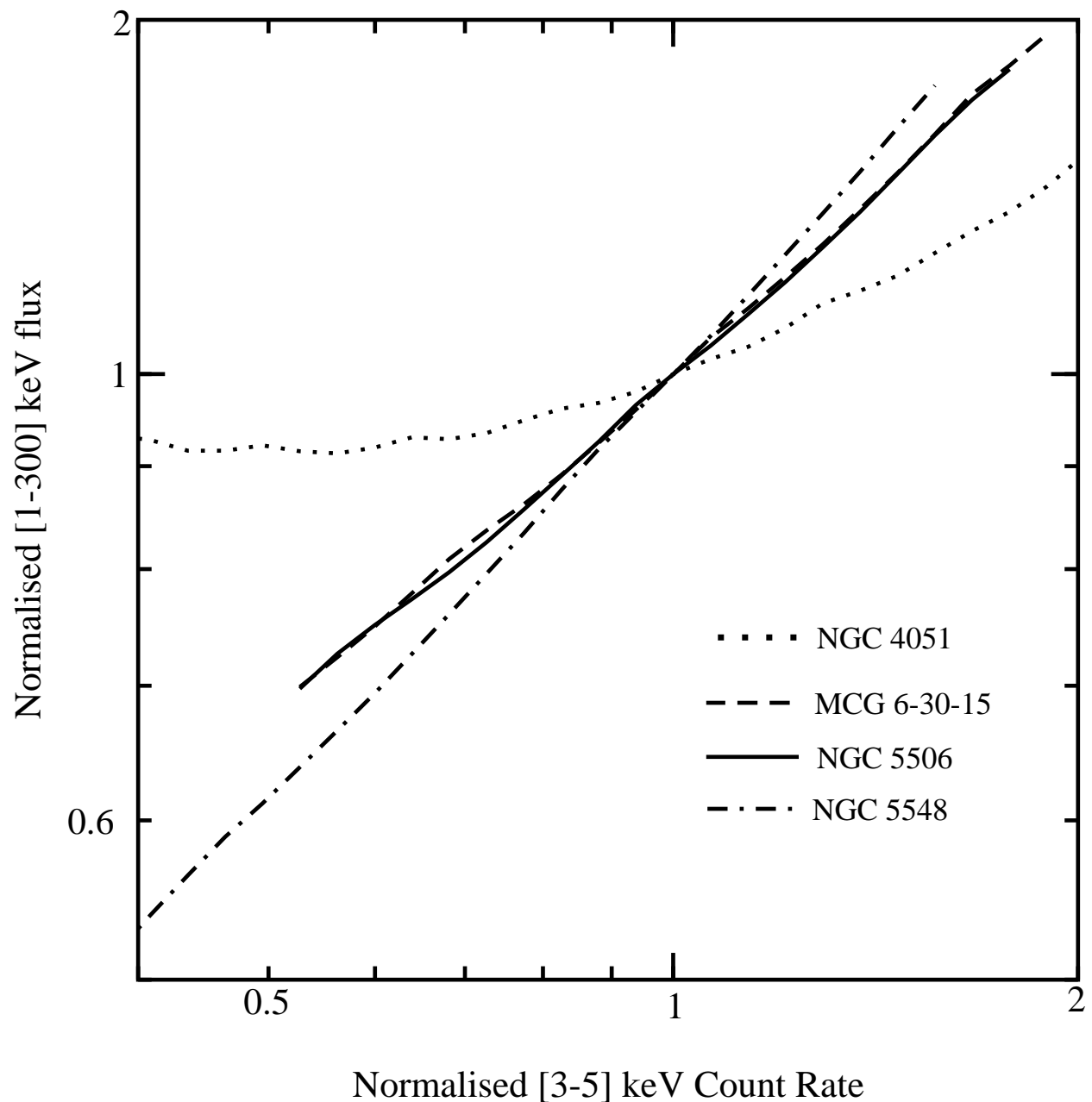


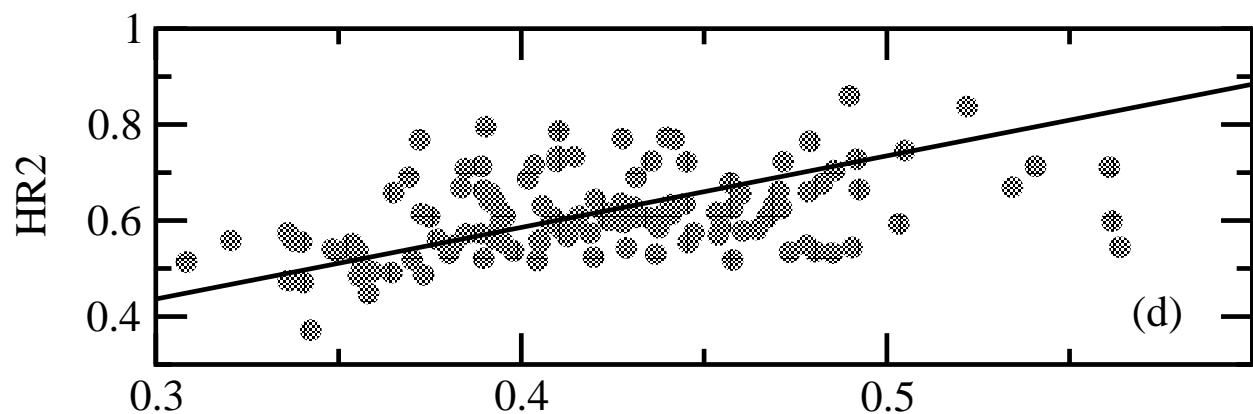
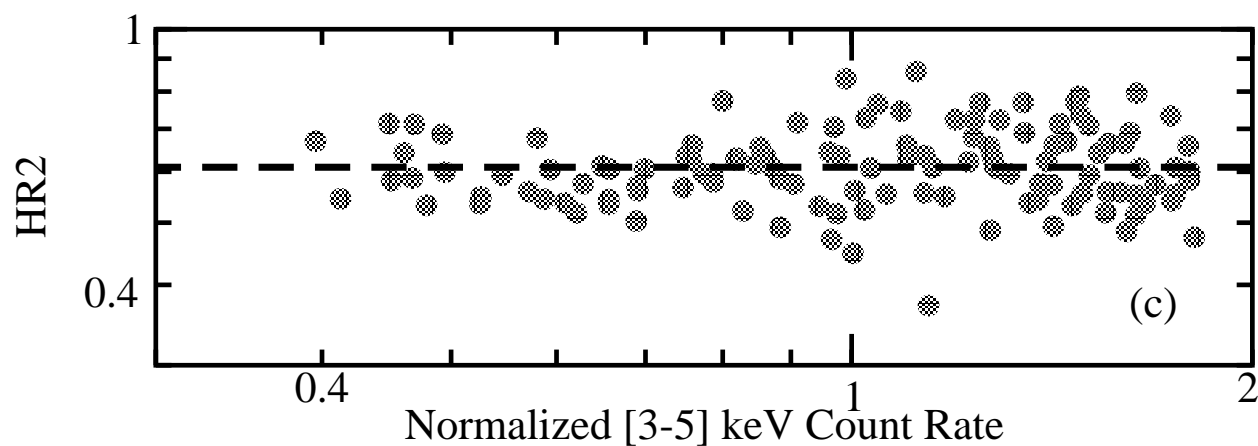
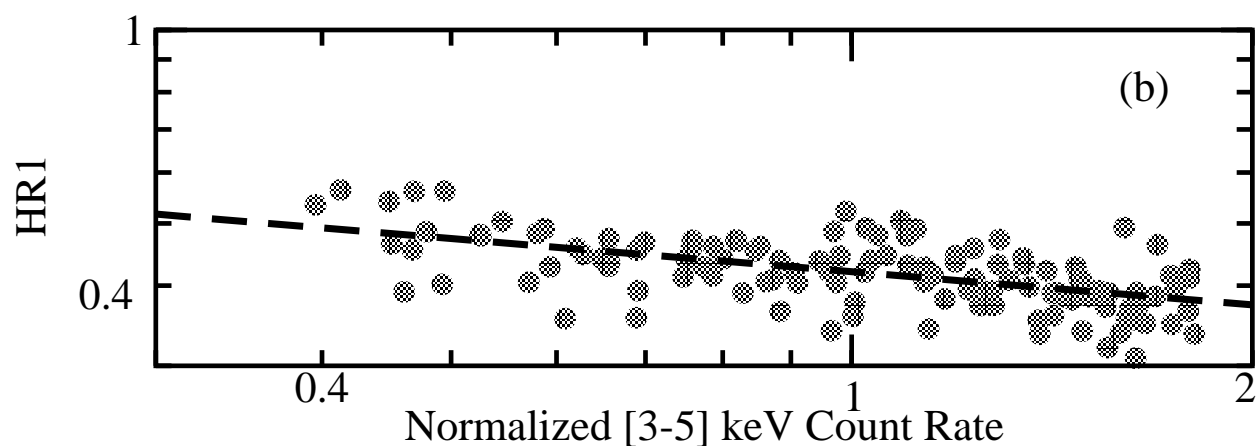
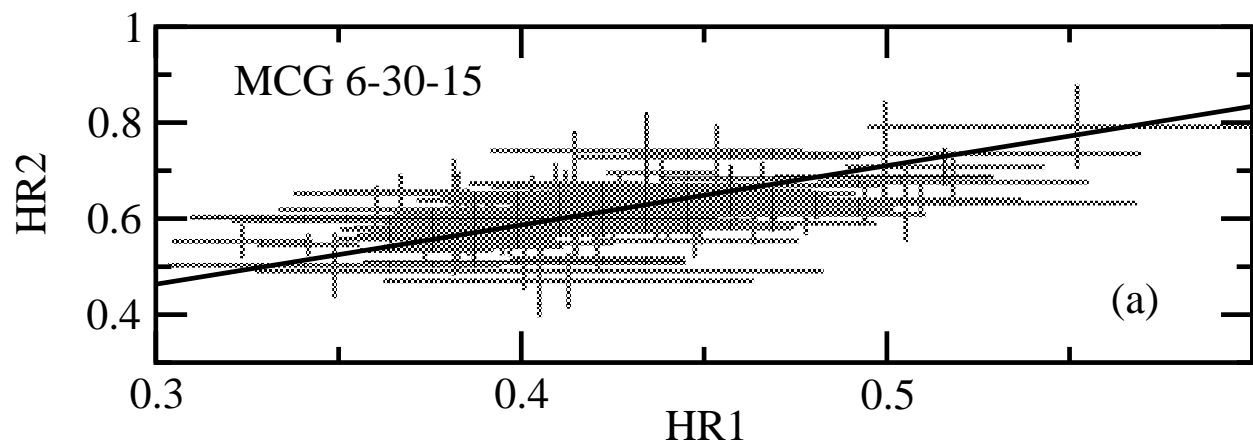


Normalized [3-5]+[7-10] keV CR



Normalized [3-5]+[7-10] keV CR





Name	$HR1$	$\sigma_{rms}$	$HR2$	$\sigma_{rms}$	$HR3$	$\sigma_{rms}$
NGC 4051	0.37	0.17	0.57	0.06	0.58	0.02
MCG -6-30-15	0.41	0.06	0.61	0.04	0.60	0.05
NGC 5506	0.51	0.03	0.64	0.03	0.62	0.04
NGC 5548	0.47	0.04	0.67	0.02	0.61	-

Table 1: The mean and  $\sigma_{RMS}$  values of the  $HR1$ ,  $HR2$ , and  $HR3$  light curves shown in Figure 2. The error on the mean  $HR$  values is less than 0.01.

Object Name	$HR1/C_{(3-5keV+7-10keV)_{norm}}$ $b_1 (\chi^2/\text{dof})$	$HR2/C_{(3-5keV)_{norm}}$ $b_1 (\chi^2/\text{dof})$	$HR3/C_{(3-5keV)_{norm}}$ $b_1 (\chi^2/\text{dof})$
NGC 4051	$-0.30 \pm 0.02(284/123)$	$-0.05 \pm 0.01(189/123)$	$-0.17 \pm 0.02(124/123)$
MCG -6-30-15	$-0.16 \pm 0.02(256/122)$	$+0.02 \pm 0.02(190/122)$	$-0.13 \pm 0.03(132/122)$
NGC 5506	$-0.10 \pm 0.01(293/125)$	$-0.01 \pm 0.01(193/125)$	$-0.10 \pm 0.01(130/125)$
NGC 5548	$-0.13 \pm 0.01(290/132)$	$+0.01 \pm 0.01(191/132)$	$-0.06 \pm 0.02(110/132)$

Table 2: Best power law model fitting results to the color-flux plots shown in Figures 3, 4 and 5.

Name	$\langle \Gamma \rangle$	$\langle R \rangle$	$\langle EW \rangle$ (eV)
NGC 4051	2.06	1.7	310
MCG -6-30-15	2.05	1.2	180
NGC 5506	2.11	1.4	230
NGC 5548	1.88	0.8	130

Table 3: The mean spectral index, reflection normalization  $R$  and iron line equivalent width ( $EW$ ) of the sources in our sample, computed using the mean hardness ratio values and a power law plus reflection and a narrow Gaussian line spectral model (see Section 4.2.1).

Name	$HR2/C_{(3-5keV)norm}$	$HR3/C_{(3-5keV)norm}$		
	$b_{CEW}$	$b_{CLF}$	$b_{CR}$	$b_{CRF}$
NGC 4051	-0.14	-0.03	-0.13	-0.15
MCG -6-30-15	-0.08	-0.02	-0.08	-0.11
NGC 5506	-0.04	-0.02	-0.05	-0.09
NGC 5548	-0.06	-0.03	-0.06	-0.09

Table 4: The slope of the model curves shown in Figures 4 and 5.  $b_{CEW}$  and  $b_{CLF}$  represent the slope of the model curves under the assumption of constant line's  $EW$  and flux respectively. Similarly,  $b_{CR}$  and  $b_{CRF}$  denote the slope of the model curves in the case of constant  $R$  and constant reflection flux respectively.